Supporting Information

Coarse-grained molecular dynamics simulations of mixtures of polysulfamides

Jay Shah[1], Arthi Jayaraman[1,2,3] *

1. Department of Chemical and Biomolecular Engineering, University of Delaware, Colburn Lab, 150 Academy Street, Newark, DE 19716

2. Department of Materials Science and Engineering, University of Delaware, 201 DuPont Hall, Newark, Delaware 19716

3. Data Science Institute, University of Delaware, Ammon Pinizzotto Biopharmaceutical Innovation Center, Suite 147, 590 Avenue 1743, Newark, DE 19713

*Corresponding author

(A.J.) arthij@udel.edu

Table of Contents

Section – 1: Details of Atomistic Simulations

► **Chemical species** are categorized into two types: those for the carbon backbone and sulfamide group.

Carbon backbone –

a. CCF: Consists of a methyl (CH_3) group followed by a methylene (CH_2) group, representing the initial segment of the chain.
b. CCL: Comprises a methyl (CH_3) group followed by a methylene (CH_2) group, representing the terminal segment of the chain.
c. CCA - residue comprises two methylene (CH_2) groups, representing the intermediate section of the backbone.

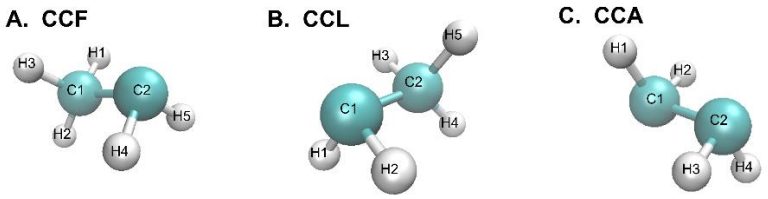

Figure S1: represents the three distinct kinds of carbon backbone species used in the simulations. (A) CCF: Consists of a methyl (CH_3) group followed by a methylene (CH_2) group. (B) CCL: Comprises a methyl (CH_3) group followed by a methylene (CH_2) group. (C) CCA: This is made up of two CH_2 groups.

Table S1*:* Details of the OPLS-AA parameters corresponding to the carbon backbone chemical species.

A. CCF

Name	OPLS-AA	Mass	Charge
C1	opls_135	12	-0.18
H1	opls_140	1	0.06
H2	opls_140	1	0.06
H3	opls_140	1	0.06
C2	opls_136	12	-0.12
H4	opls_140	1	0.06
H5	opls_140	1	0.06

B. CCL

Name	OPLS-AA	Mass	Charge
C1	opls_136	12	-0.12
H1	opls_140	1	0.06
H2	opls_140	1	0.06
C2	opls_135	12	-0.18
H3	opls_140	1	0.06
H4	opls_140	1	0.06
H5	opls_140	1	0.06

C. CCA

Name	OPLS-AA	Mass	Charge
C1	opls_136	12	-0.12
H1	opls_140	1	0.06
H2	opls_140	1	0.06
C2	opls_136	12	-0.12
H3	opls_140	1	0.06
H4	opls_140	1	0.06

Sulfamide group

The sulfamide group consists of two carbon atoms adjacent to the sulfamide group, known as the alpha and beta carbons. These carbons have slightly different charges than the other carbons in the backbone. **SUL** includes the sulfamide group along with the alpha and beta carbons in the backbone. **Figure S2** and **Table S2** present the schematic and details the OPLS-AA parameters for these atoms. Although the OPLS-AA parameters are designed for sulfonamides rather than sulfamides, they are applicable here, with the main distinction being that one of the N-H groups in sulfamide is replaced by a radical in sulfonamides.

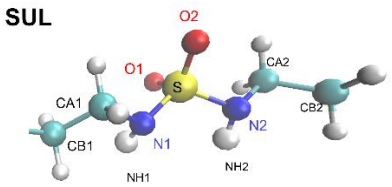

Figure S2: represents **SUL** group along with their naming convention.

Table S2: Details of the OPLS-AA parameters corresponding to the sulfamide species.

SUL

Name	OPLS-AA	Mass	Charge
CB1	OPLS_486	12	-0.18
HB1	OPLS_487	1	0.06
HB2	OPLS_487	1	0.03
CA1	OPLS_482	12	0.18
HA1	OPLS_483	1	0.03
HA2	OPLS_483	1	0.03
N1	OPLS_480	14	-0.8
NH1	OPLS_481	1	0.41
S	OPLS_474	32	1.480
O1	OPLS_475	16	-0.68
O2	OPLS_475	16	-0.68
N2	OPLS_480	14	-0.8
NH2	OPLS_481	1	0.41
CA2	OPLS_482	12	0.18
HA3	OPLS_483	1	0.03
HA4	OPLS_483	1	0.03
CB2	OPLS_486	12	-0.18
HB3	OPLS_487	1	0.06
HB4	OPLS_487	1	0.03

Figure S3 A and B, shows the different nomenclature associated with the CCA and SUL groups, respectively, to highlight the connectivity variations within the molecular structure. Despite alterations in naming convention and connectivity, it is worth noting that the OPLS-AA parameters remain consistent for similar groups.

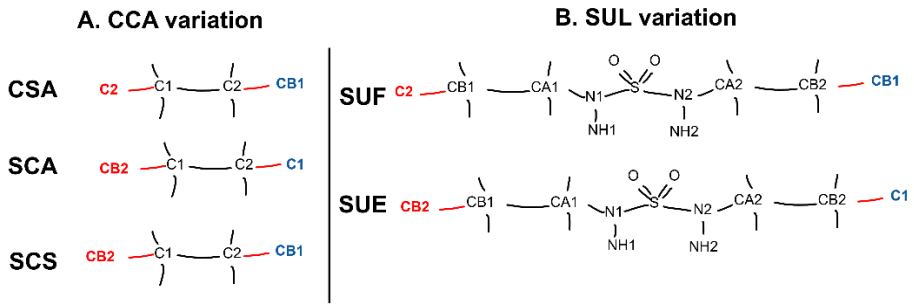

Figure S3: (A) Variations in nomenclature for the CCA group based on its connection with the sulfamide group in the backbone. (B) Variations in nomenclature for the SUL group based on its connection with the carbon group in the backbone.

►Angle and Dihedral Parameters

Since the OPLS-AA parameters are not specifically designed for sulfamide, certain angle and dihedral parameters involving sulfur and both nitrogens are not included in the ffbonded.itp file. We have supplemented these values with the closest approximations available.

Angle in OPLS-AA parameter is modeled as harmonic potential.

$$V_{angle} = \sum_{angles} k_{\theta}(\theta - \theta_0)^2$$

Dihedral in OPLS-AA parameter is modeled via Ryckaert-Bellemans potential.

$$V_{dihedral} = \sum_{n=1}^{5} C_n \cos^n \psi$$

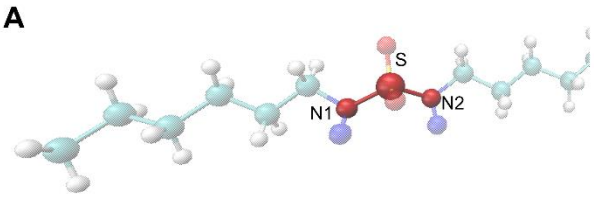

Angle parameter

θ_0	k_θ
111.5	850

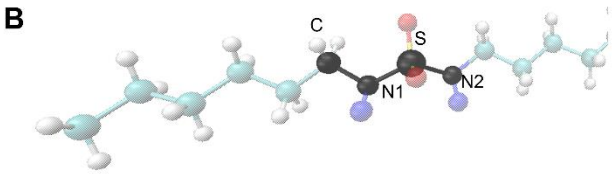

Dihedral parameter

C_0	C_1	C_2	C_3	C_4	C_5
0.0628	-4.198	3.2133	0.97905	0	0

Figure S4: (A) highlights the angle that was missing; the parameters are taken from the angle observed in small molecule sulfamide as per Gong et al.[2] (B) highlights the dihedral that was missing; we adopted the (C-C-N-S) dihedral value as the most suitable approximation available.

Section – 2: Atomistic Simulations Results

Results for polysulfamide [4,8] and polysulfamide [2,10]

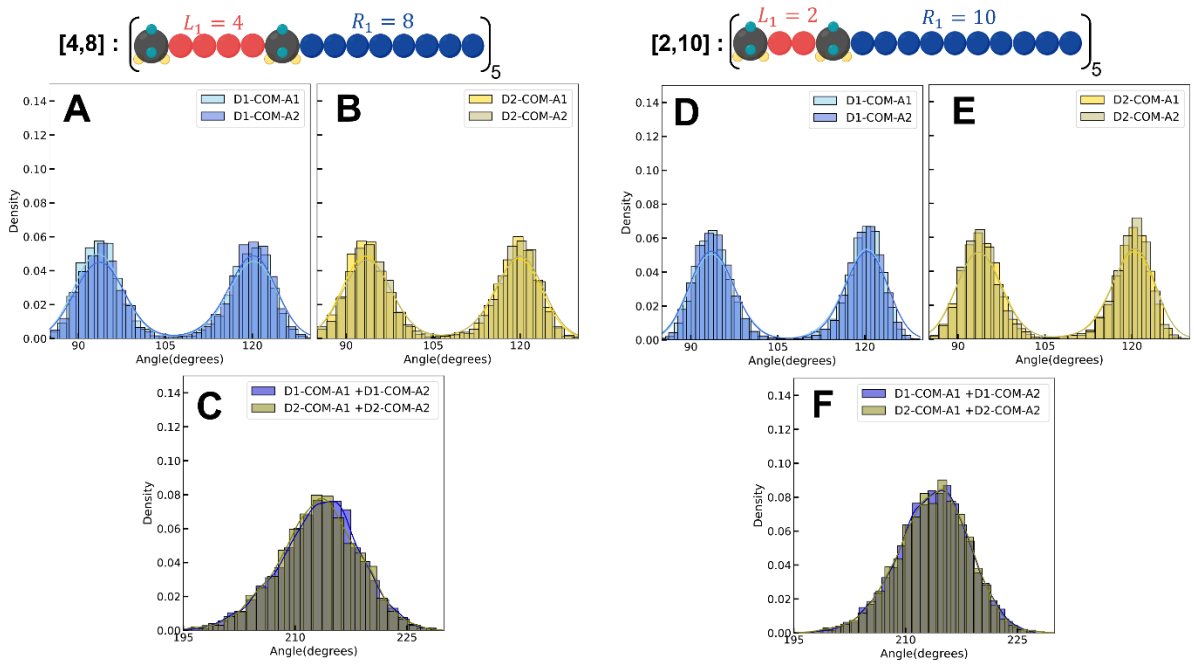

Figure S5: For [4,8] polysuflamide (A) displays the angle distribution of D1–COM–A1 and D1–COM–A2 for all sulfamide groups in the chain, (B) shows the angle distribution of D2–COM–A1 and D2–COM–A2, and (C) presents the angle distribution of the sum of the angles D1–COM–A1 and D1–COM–A2. For comparison, the histogram for the sum of angles D2–COM–A1 and D2–COM–A2 is also shown, derived from two hundred configurations across three independent trials. For [2,10] polysuflamide (D) displays the angle distribution of D1–COM–A1 and D1–COM–A2 for all sulfamide groups in the chain, (E) shows the angle distribution of D2–COM–A1 and D2–COM–A2, and (F) presents the angle distribution of the sum of the angles D1–COM–A1 and D1–COM–A2. For comparison, the histogram for the sum of angles D2–COM–A1 and D2–COM–A2 is also shown, derived from two hundred configurations across three independent trials.

Section – 3: Comparing Morphologies Observed in Simulations Using the Older CG Model of Wu Et al. Vs Atomistically-Informed CG Model

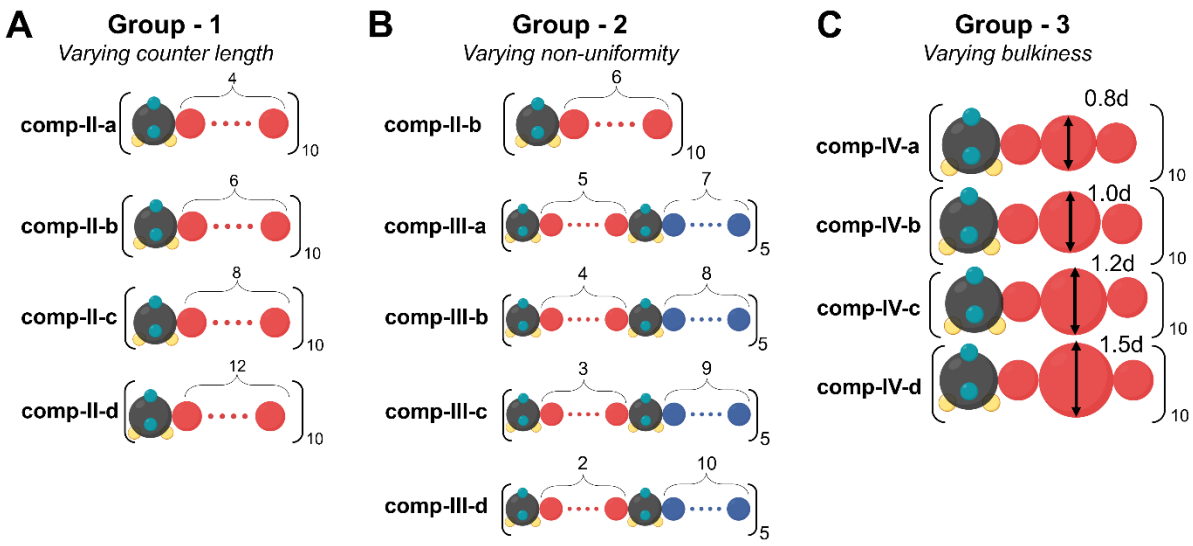

Figure S6: CG model representations for the three groups of homopolymers studied: (A) Systems with varying contour lengths, from the shortest (comp-II-a) to the longest (comp-II-d). (B) Systems varying in non-uniformity of segment choice, from the most uniform chain (comp-II-a) to the most non-uniform chain (comp-III-c). (C) Systems with increasing bulkiness, from the least bulky (comp-IV-a) to the bulkiest (comp-IV-d).

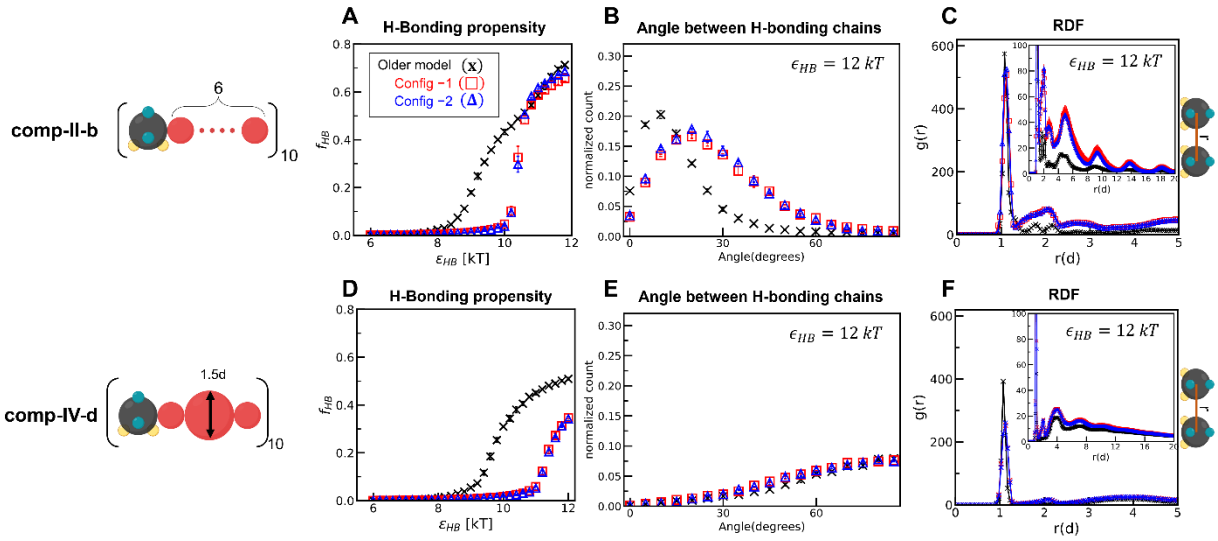

Figure S7: CG model comparison between older model, atomistically-informed Config-1 and Config-2 model for comp-II-b (A) H-Bonding propensity (B) Angle between H-bonding chains (C) radial distribution function between sulfamide groups. And for comp-IV-d (D) H-Bonding propensity (E) Angle between H-bonding chains (F) radial distribution function between

sulfamide groups. For the analyzed values, we compute the mean across ten configurations for each trial and report mean and standard deviation of the three-trial means.

► **Group 1:** different aliphatic chain contour lengths in the computational polymer systems labeled comp-II-a to comp-II-d

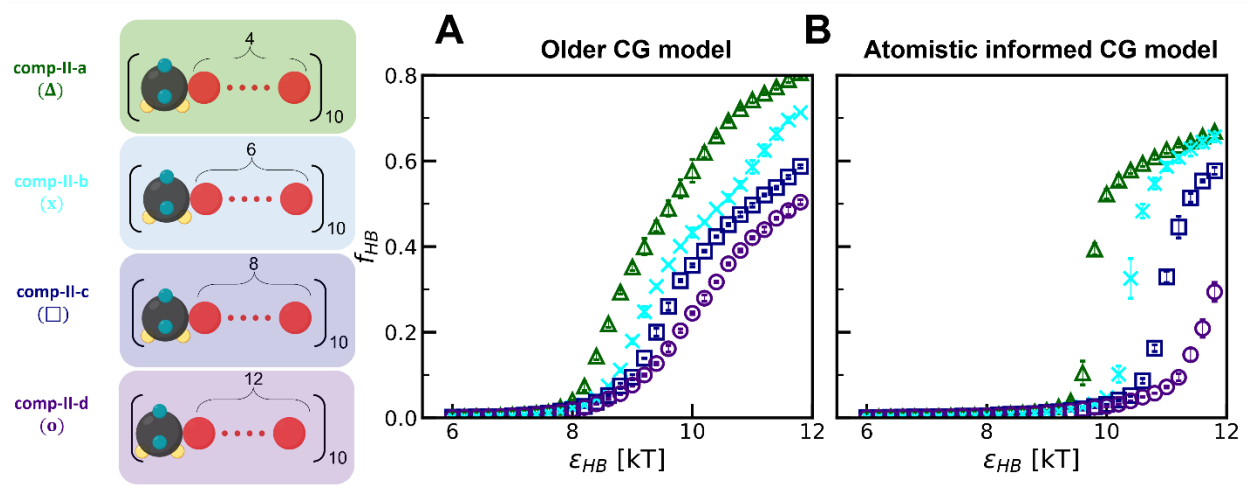

Figure S8: H-bonding propensity (f_{HB}) for comp-II-a to comp-II-d at ϵ_{HB} = 6−12 kT in simulations using the (A) Older CG model (B) Atomistic informed CG Config -1 model. For each simulation, we compute the H-bonding propensity from ten configurations collected. Error bars represent the standard deviation of these means across the three independent trials.

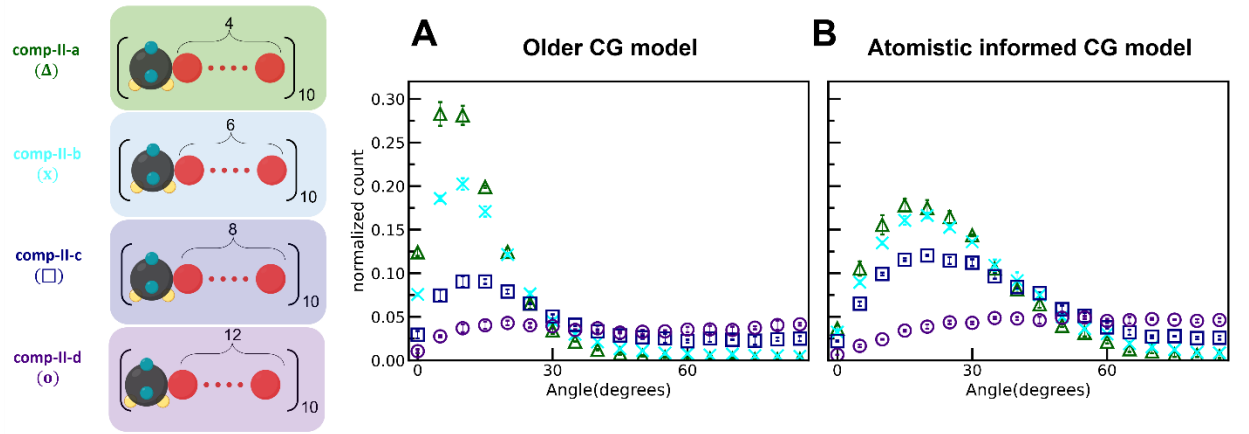

Figure S9: Distribution of angle between the H-bonding chains for comp-II-a to comp-II-d at ϵ_{HB} =12kT (A) Older CG model (B) Atomistic informed CG Config -1 model. For each simulation, we compute the distribution of angles between the H-bonding chains from ten configurations collected. Error bars represent the standard deviation of these means across the three independent trials.

►**Group 2:** Polysulfamides in comp-II-a and comp-III-a through comp-III-d have the same total number of 12 alkyl carbons in each repeating unit but vary in the lengths of the alkyl chains on either side of the sulfamide group.

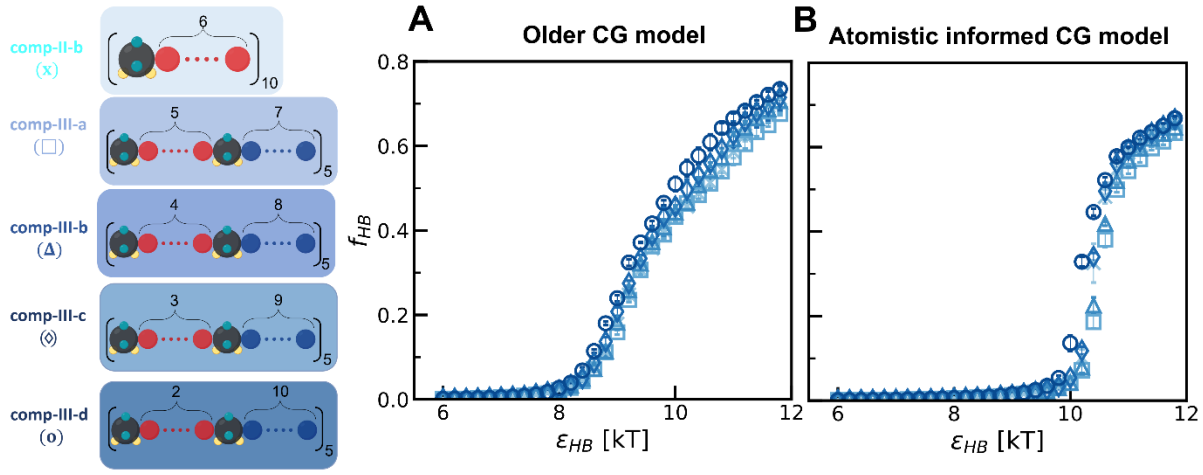

Figure S10: H-bonding propensity (f_{HB}) for comp-II-b, comp-III-a to comp- III-d at ϵ_{HB} = 6−12 kT in simulations using the(A) Older CG model (B) Atomistic informed CG Config -1 model. For each simulation, we compute the H-bonding propensity from ten configurations collected. Error bars represent the standard deviation of these means across the three independent trials.

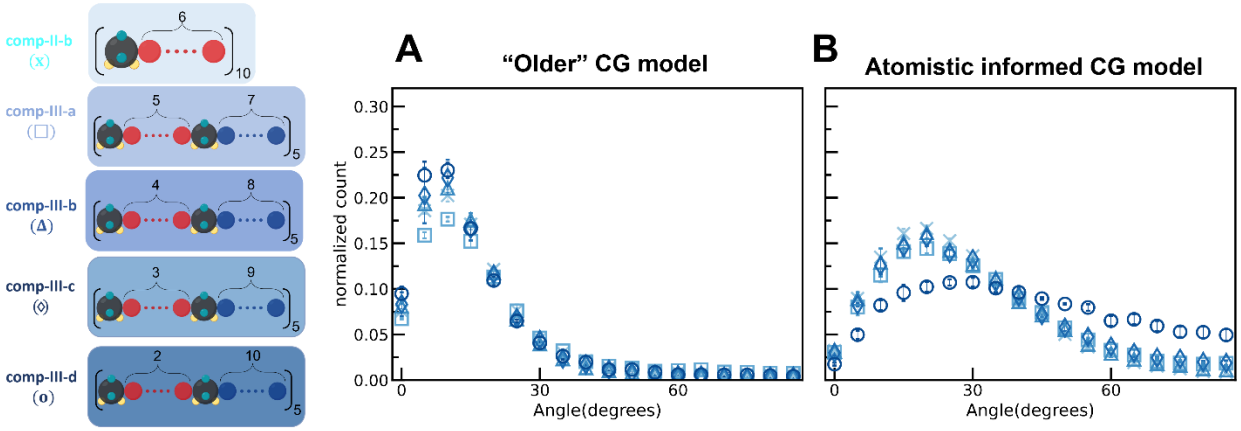

Figure S11: Distribution of angle between the H-bonding chains for comp-II-b, comp-III-a to comp- III-d at ϵ_{HB} =12kT (A) Older CG model (B) Atomistic informed CG Config -1 model. For each simulation, we compute the distribution of angles between the H-bonding chains from ten configurations collected. Error bars represent the standard deviation of these means across the three independent trials.

►**Group 3:** Increasing bulkiness of the coarse-grained (CG) beads going from comp-IV-a to comp-IV-d. We systematically vary the diameters of these bulky group beads relative to the smaller beads representing the −CH2− groups in the repeating unit, ranging from 0.8d to 1.5d. Corresponding real structures synthesized by Wu et al. are presented in that paper.

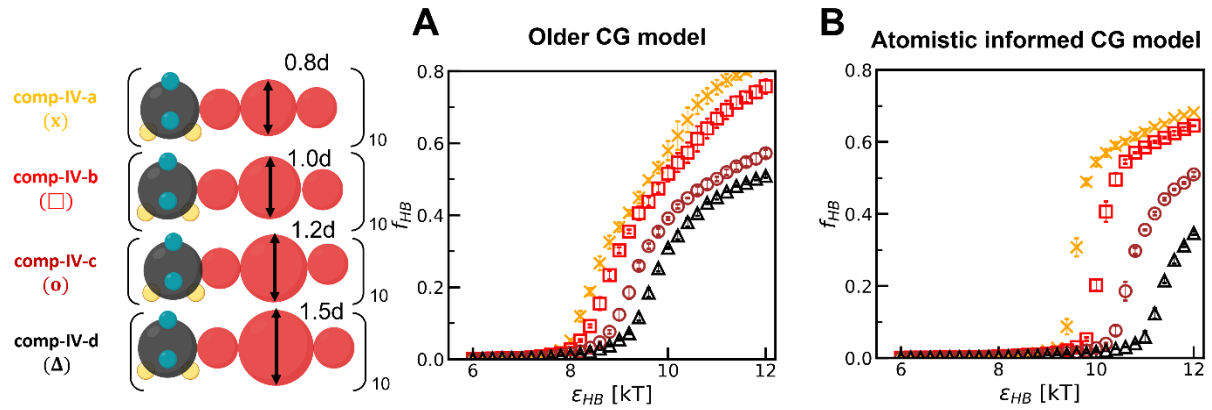

Figure S12: H-bonding propensity (f_{HB}) for comp-IV-a to comp-IV-d at ϵ_{HB} = 6−12 kT in simulations using the(A) Older CG model (B) Atomistic informed CG Config -1 model. For each simulation, we compute the H-bonding propensity from ten configurations collected. Error bars represent the standard deviation of these means across the three independent trials.

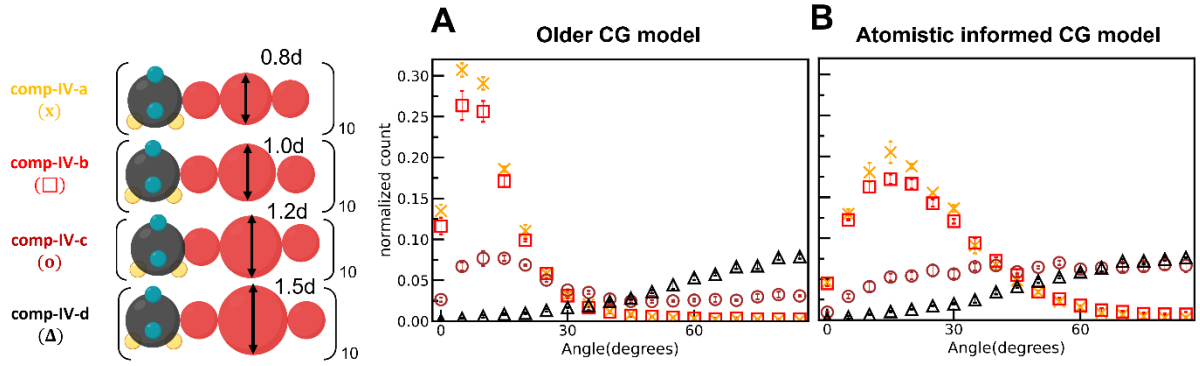

Figure S13: Distribution of angle between the H-bonding chains for comp-IV-a to comp-IV-d at ϵ_{HB} =12kT (A) Older CG model (B) Atomistic informed CG Config -1 model. For each simulation, we compute the distribution of angles between the H-bonding chains from ten configurations collected. Error bars represent the standard deviation of these means across the three independent trials.

Section – 4: Additional Figures for Coarse-Grained Molecular Dynamics Simulation

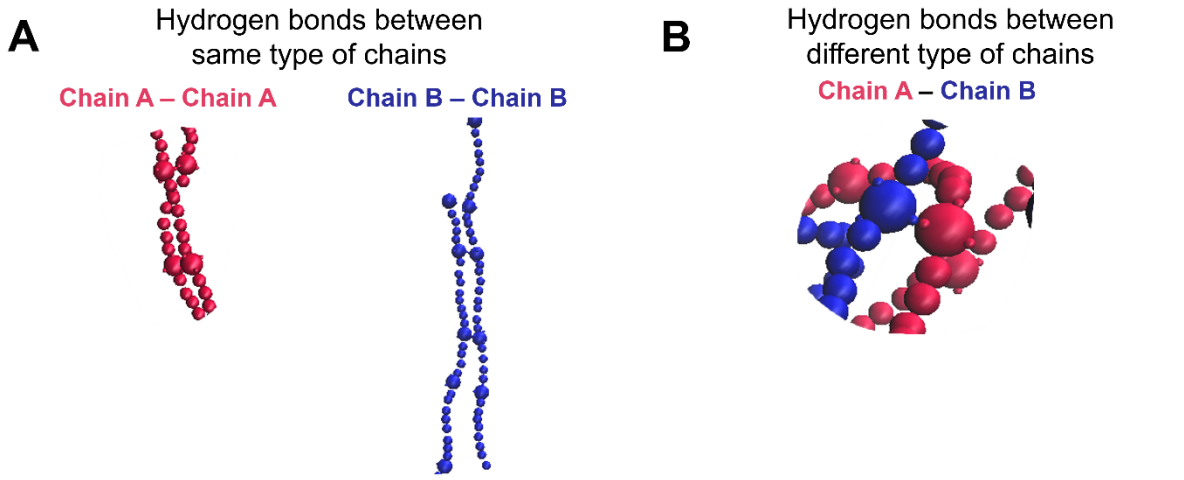

Figure S14 H-bonding interactions between (A) chains of the same type (B) chains of distinct types within the mixture.

Section – 5: Additional Results from Mixtures with Varying Segment Lengths

► **Using Atomistic-informed model (Figures S15 – S17)**

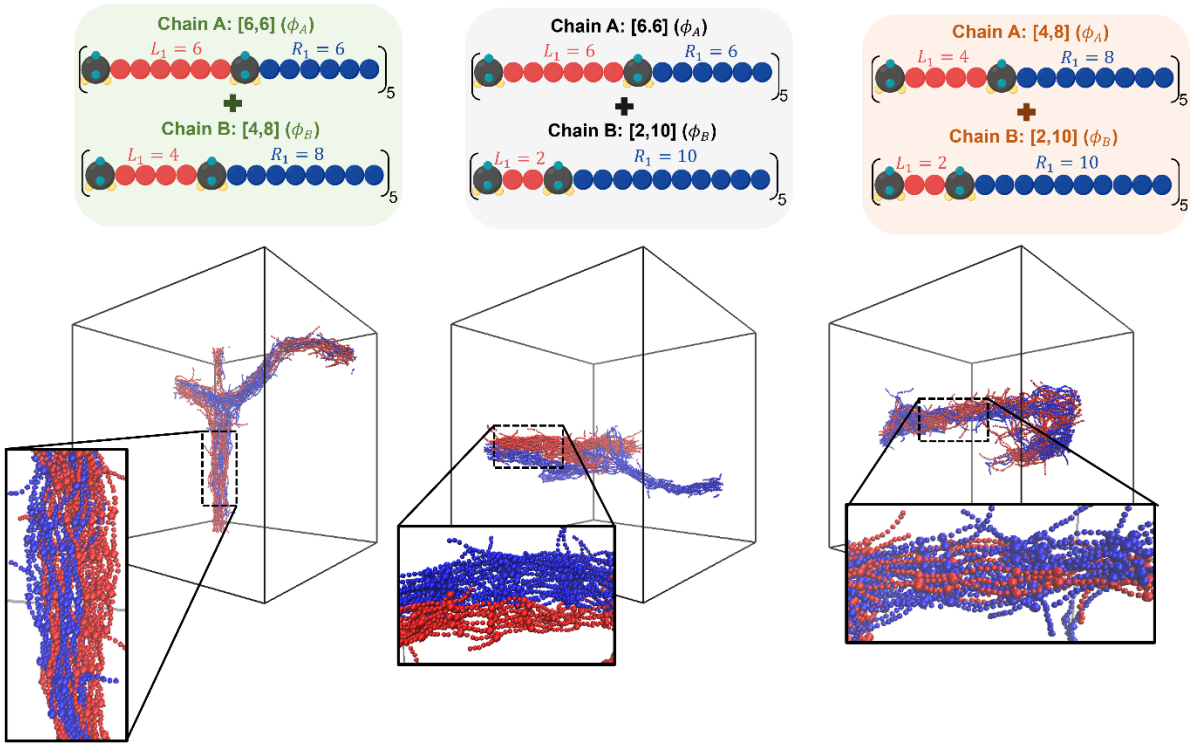

Figure S15: Simulations snapshots of the three mixtures (A) [6,6] + [4,8] (B) [6,6] + [2,10] and (C) [4,8] + [2,10] at mixture compositions of 50:50 at $\epsilon_{HB} = 12\ kT$.

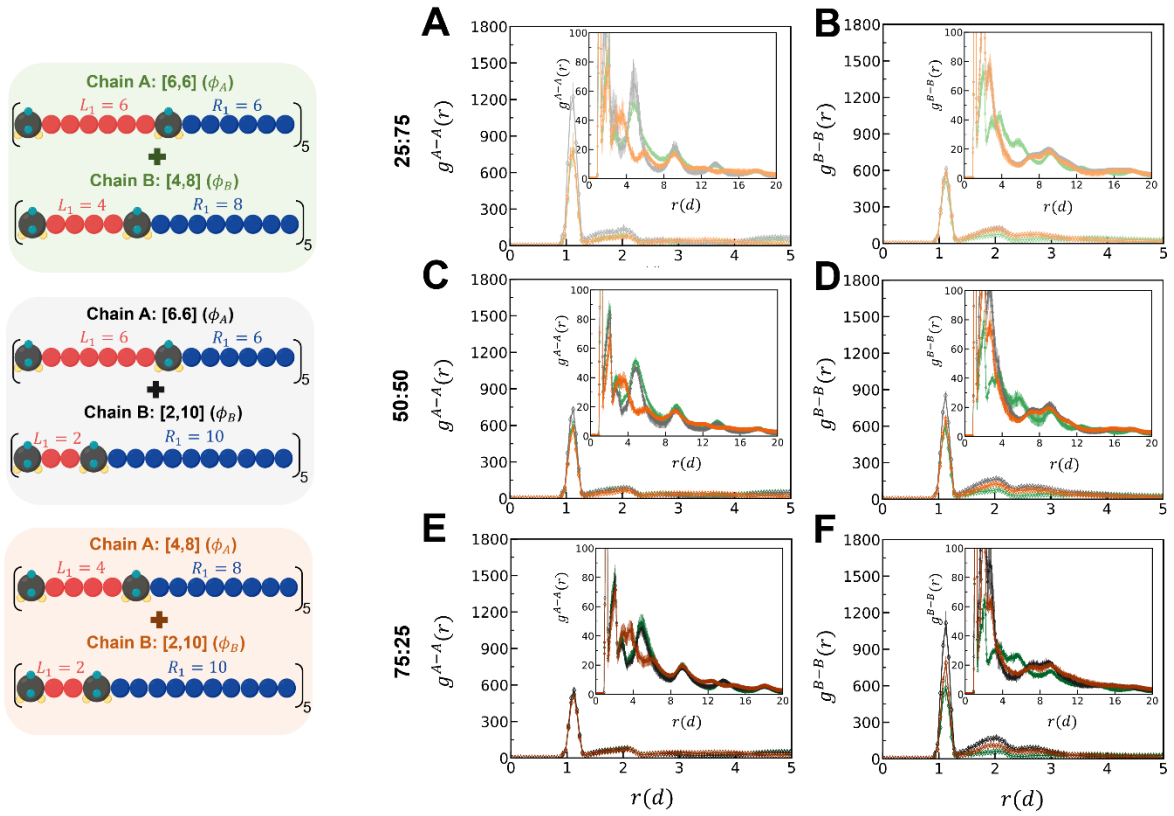

Figure S16: Sulfamide-sulfamide RDFs using *Atomistic informed CG Config -1 model* at different mixture compositions: (A, B) at 25:75, (C, D) at 50:50, and (E, F) at 75:25 at ϵ_{HB} = 12 kT. (A, C, E) shows $g^{A-A}(r)$ while (B, D, F) show $g^{B-B}(r)$. The green shading represents the mixture of [6,6] and [4,8], the grey shading represents [6,6] and [2,10], and the orange shading represents [4,8] and [2,10]. For each simulation, we compute the RDFs from ten configurations collected. Error bars represent the standard deviation of these means across the three independent trials.

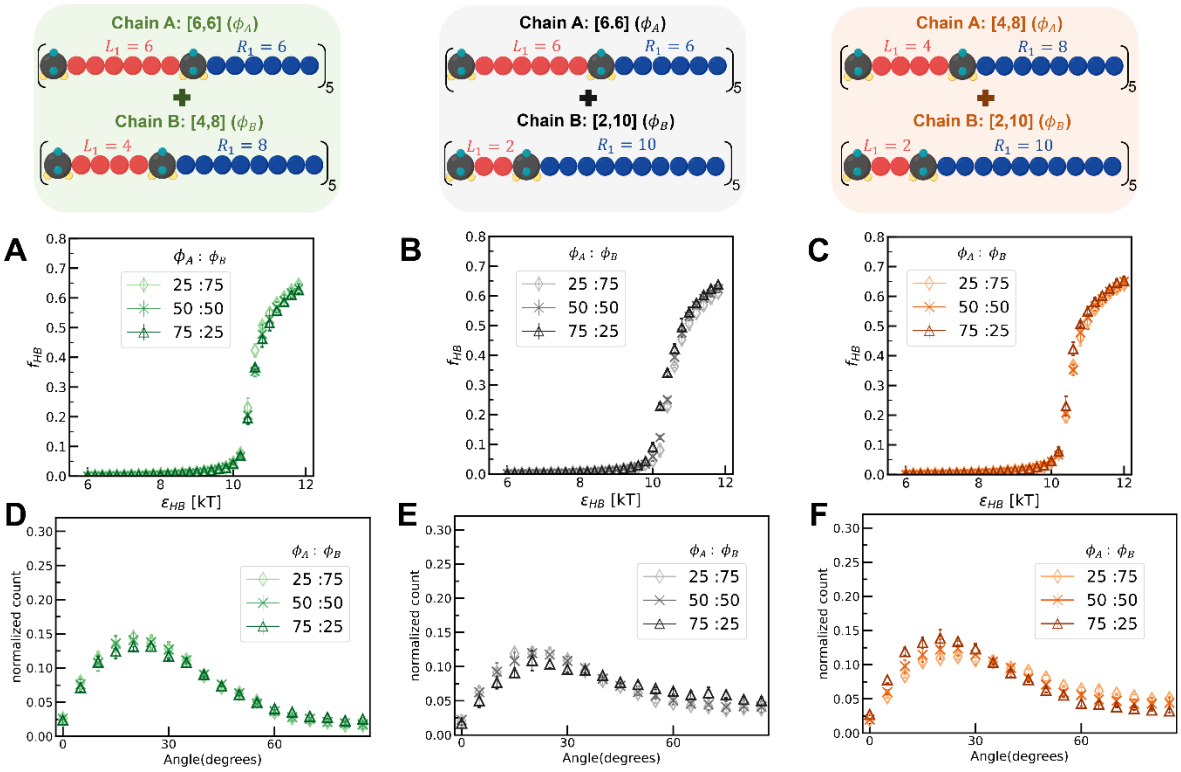

Figure S17: H-bonding propensity (f_{HB}) for the three mixtures (A) [6,6] and [4,8] (B) [6,6] and [2,10] (C) [4,8] and [2,10] across the mixture compositions of 25:75, 50:50, and 75:25 at ϵ_{HB} = 6−12 kT in simulations using the *Atomistic informed CG Config -1 model*. For each simulation, we compute the H-bonding propensity from ten configurations collected. Error bars represent the standard deviation of these means across the three independent trials.

Distribution of angle between the H-bonding chains for the three mixtures (D) [6,6] and [4,8] (E) [6,6] and [2,10] (F) [4,8] and [2,10] across the mixture compositions of 25:75, 50:50, and 75:25 at ϵ_{HB} =12kT using the *Atomistic informed CG Config -1 model*. For each simulation, we compute the distribution of angles between the H-bonding chains from ten configurations collected. Error bars represent the standard deviation of these means across the three independent trials.

►**Using older CG model (Figures S18 – S21)**

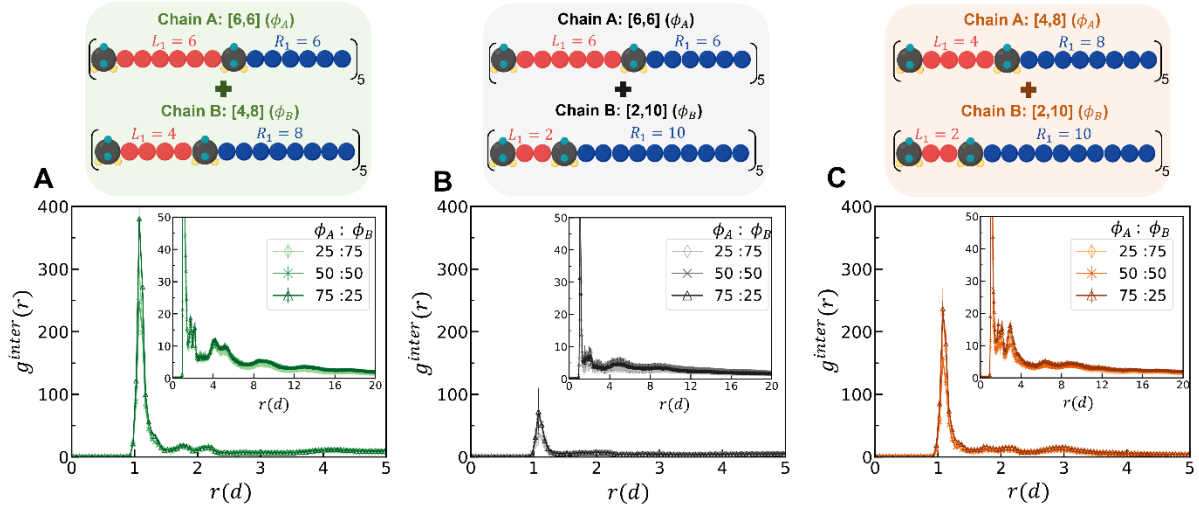

Figure S18: Inter-chain sulfamide-sulfamide RDFs ($g^{inter}(r)$) using **older CG model** for mixture of (A) [6,6] and [4,8] (B) [6,6] and [2,10] (C) [4,8] and [2,10] for mixture compositions of 25:75, 50:50 and 75:25 at ϵ_{HB} = 12 kT. Inset display $g^{inter}(r)$ (on y-axis) for r >20d (on x-axis), highlighting the long-range spatial organization. For each simulation, we compute the RDFs from ten configurations collected. Error bars represent the standard deviation of these means across the three independent trials.

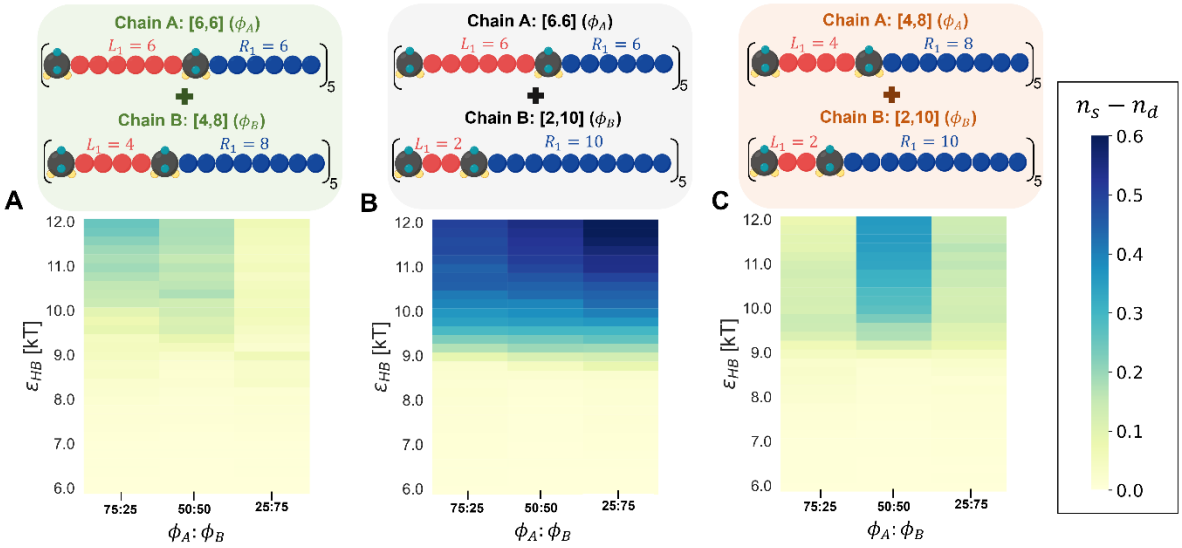

Figure S19: Heat maps showing the difference in H-bonding between identical chain types (n_s) and different chain types (n_d) using the **older CG model** for the three mixtures - (A) [6,6] and [4,8], (B) [6,6] and [2,10] and (C) [4,8] and [2,10] - at varying H-bonding strengths (y-axis) and mixture compositions (x-axis).

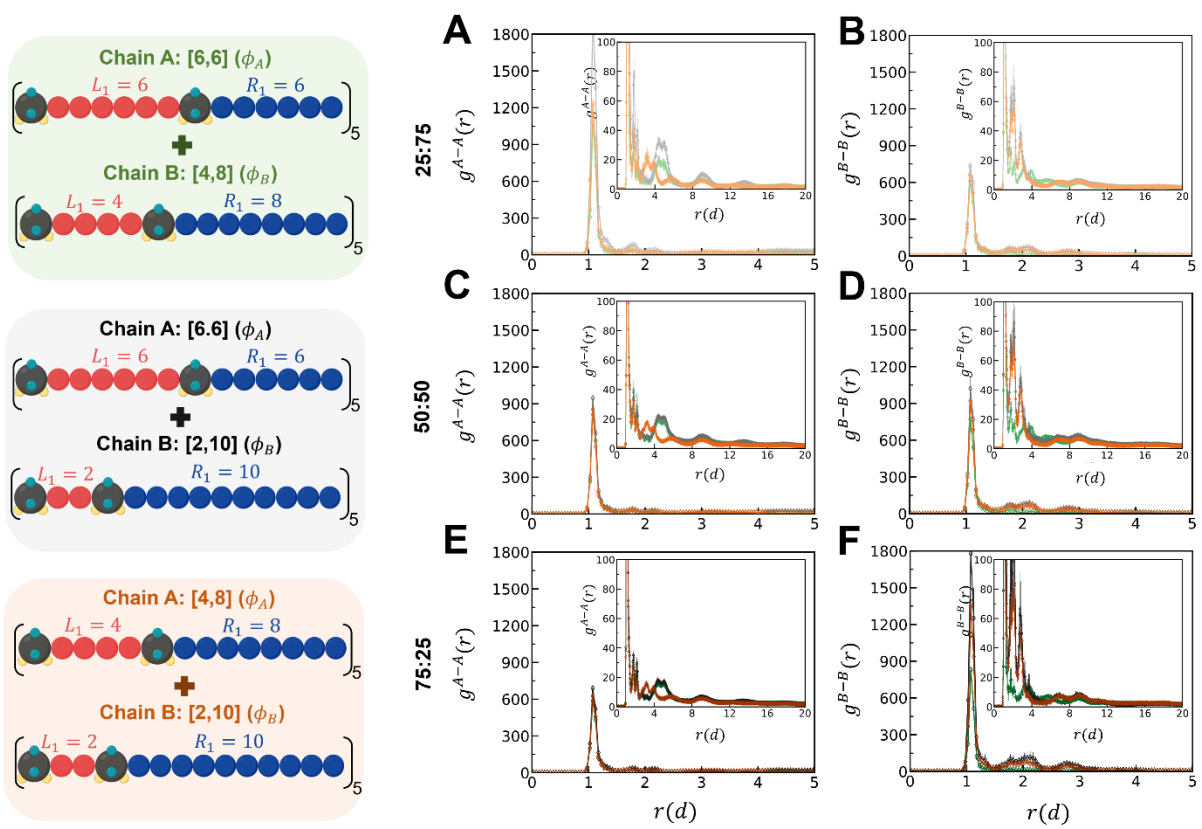

Figure S20: Sulfamide-sulfamide RDFs using the **older CG model** are shown for mixtures at different mixture compositions: (A, B) at 25:75, (C, D) at 50:50, and (E, F) at 75:25 at ϵ_{HB} = 12 kT. (A, C, E) shows $g^{A-A}(r)$ while (B, D, F) show $g^{B-B}(r)$. The green shading represents the mixture of [6,6] and [4,8], the grey shading represents [6,6] and [2,10], and the orange shading represents [4,8] and [2,10]. For each simulation, we compute the RDFs from ten configurations collected. Error bars represent the standard deviation of these means across the three independent trials.

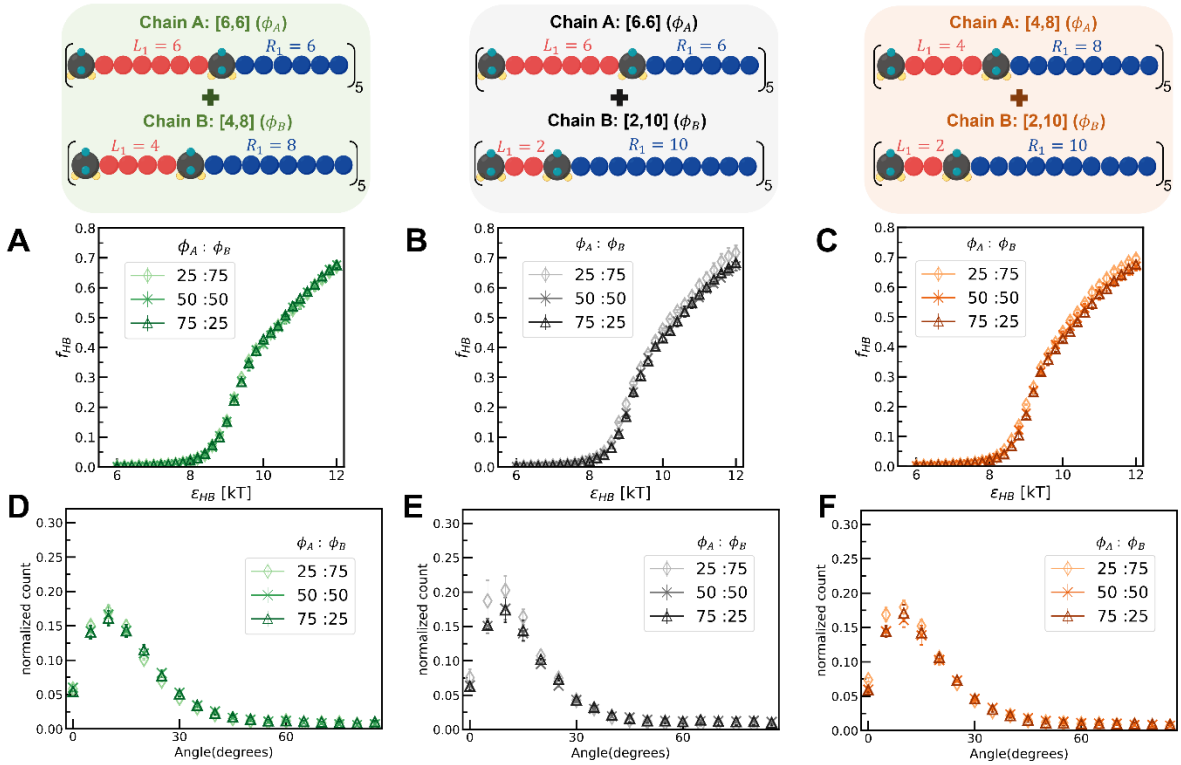

Figure S21: H-bonding propensity (f_{HB}) for the three mixtures (A) [6,6] and [4,8] (B) [6,6] and [2,10] (C) [4,8] and [2,10] across the mixture compositions of 25:75, 50:50, and 75:25 at ϵ_{HB} = 6−12 kT in simulations using the **older CG model**. For each simulation, we compute the H-bonding propensity from ten configurations collected. Error bars represent the standard deviation of these means across the three independent trials.

Distribution of angle between the H-bonding chains for the three mixtures (D) [6,6] and [4,8] (E) [6,6] and [2,10] (F) [4,8] and [2,10] across the mixture compositions of 25:75, 50:50, and 75:25 at ϵ_{HB} =12kT using the **older CG model**. For each simulation, we compute the distribution of angles between the H-bonding chains from ten configurations collected. Error bars represent the standard deviation of these means across the three independent trials.

Section – 6: Additional Results from Mixtures with Varying Bulkiness

► Using Atomistic-informed model (Figures S22 – S25)

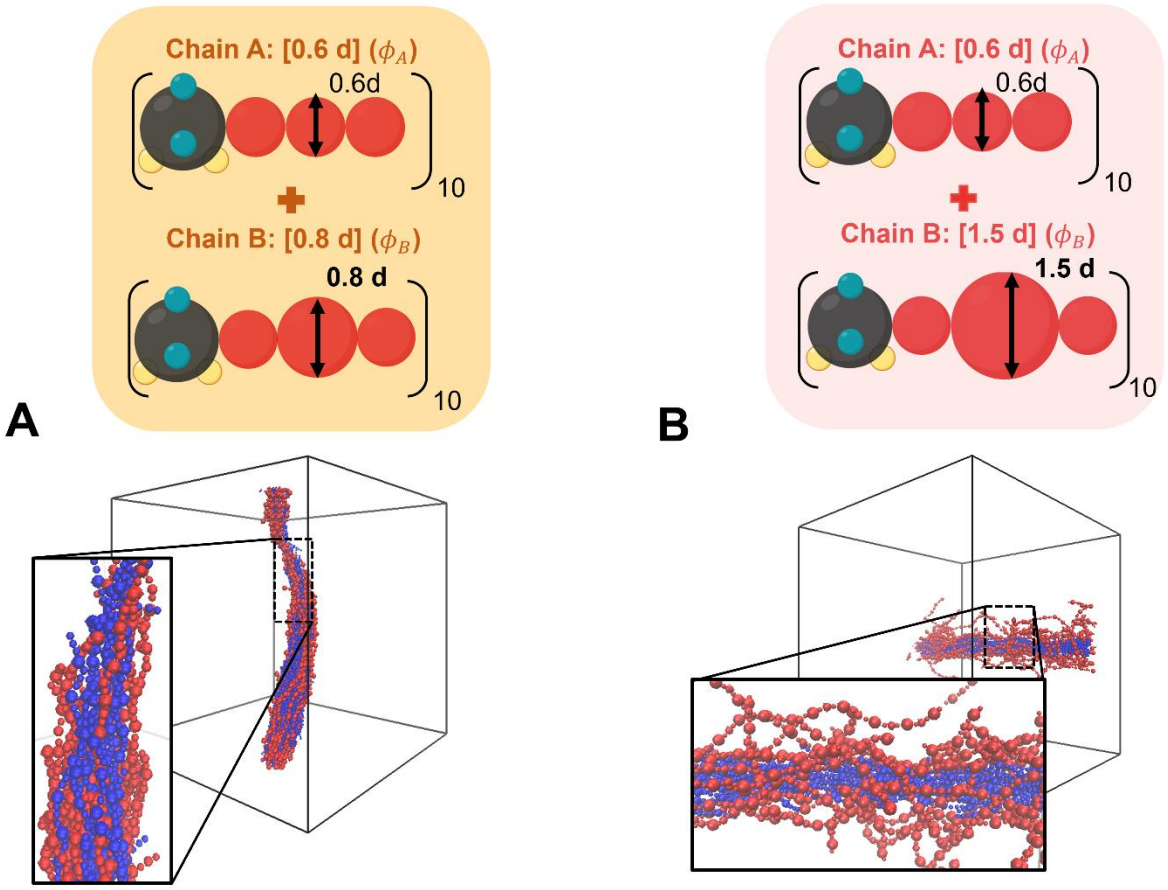

Figure S22: shows the simulations snapshot of two mixtures (A) [0.6 d] and [0.8 d] (B) [0.6 d] and [1.5 d] at the mixture compositions of 50:50 at $\epsilon_{HB} = 12\ kT$.

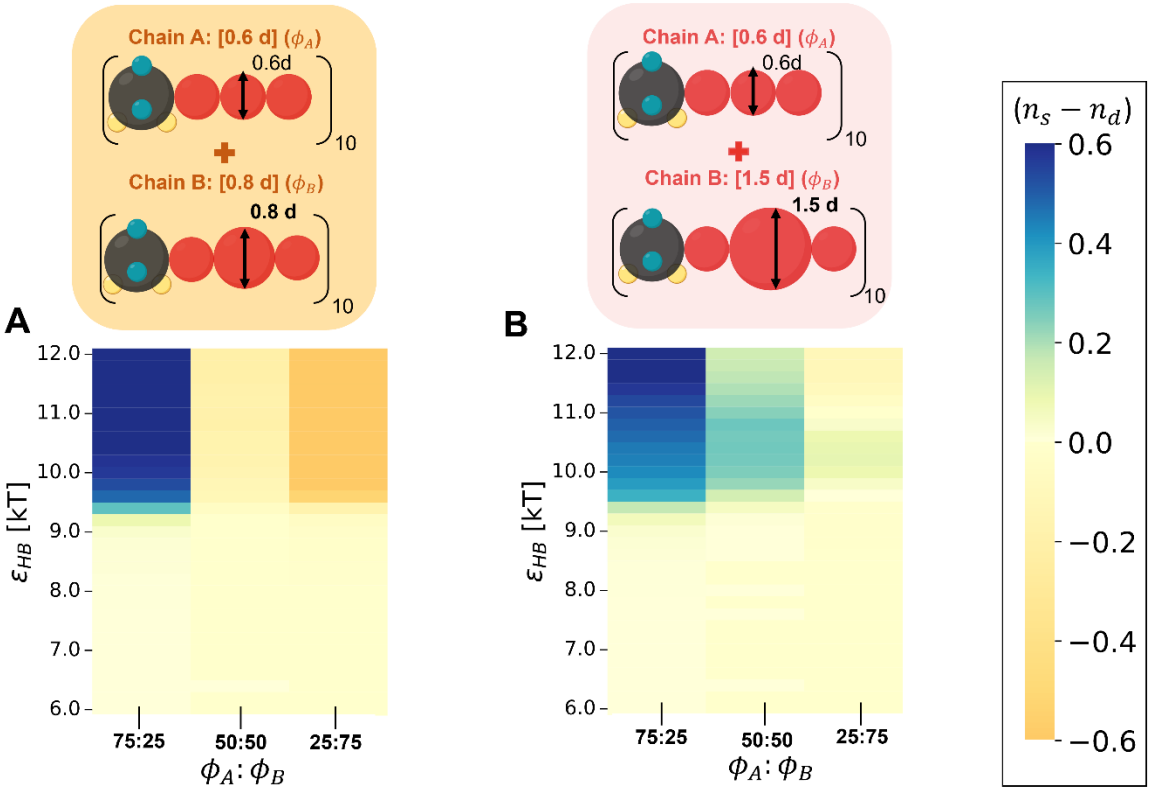

Figure S23: Heat maps showing the difference in hydrogen bonding between identical chain types (n_s) and different chain types (n_d) using the *Atomistic informed CG Config -1 model* for the two mixtures (A) [0.6 d] and [0.8 d] (B) [0.6 d] and [1.5 d] at varying H-bonding strengths (y-axis) and mixture compositions (x-axis).

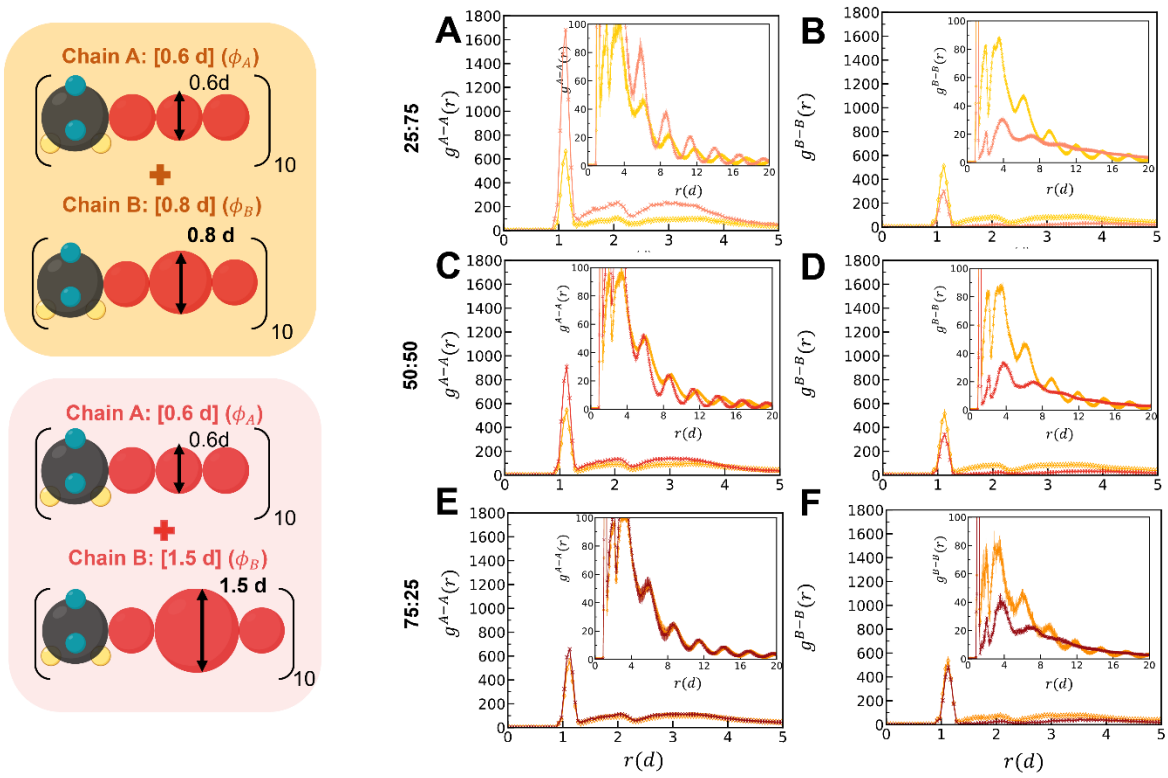

Figure S24: Sulfamide-sulfamide RDFs using the *Atomistic informed CG Config -1 model* are shown for mixtures at different mixture compositions: (A, B) at 25:75, (C, D) at 50:50, and (E, F) at 75:25 at ϵ_{HB} = 12 kT. (A, C, E) shows $g^{A-A}(r)$ while (B, D, F) show $g^{B-B}(r)$. (A, C, E) shows $g^{(A-A)}$ (r) while (B, D, F) show $g^{(B-B)}$(r). The yellow shading represents the mixture of [0.6 d] and [0.8 d], the red shading represents [0.6 d] and [1.5 d]. For each simulation, we compute the RDFs from ten configurations collected. Error bars represent the standard deviation of these means across the three independent trials.

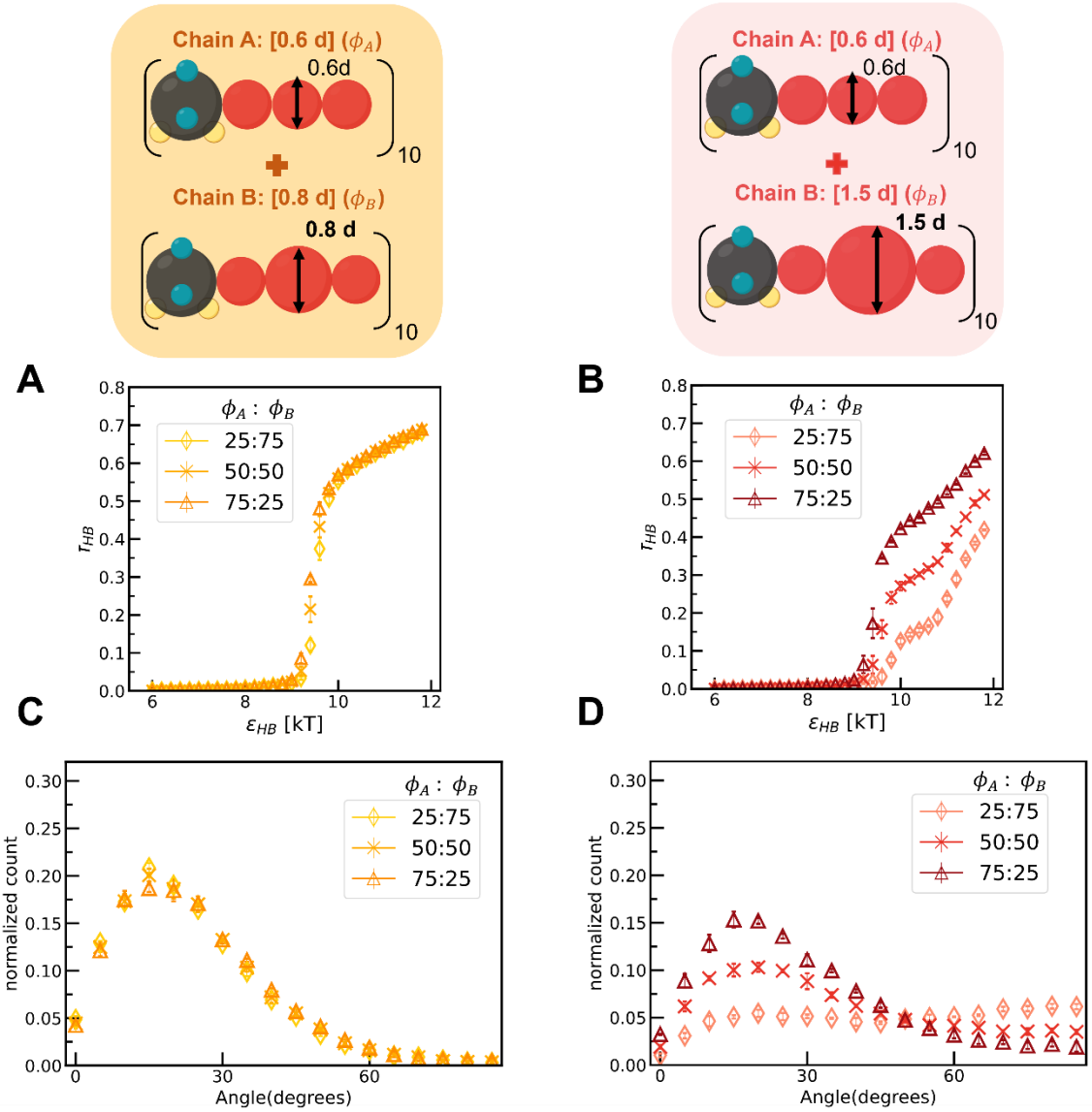

Figure S25: H-bonding propensity (f_{HB}) for mixture of: (A) [0.6 d] and [0.8 d] (B) [0.6 d] and [1.5 d] across the mixture compositions of 25:75, 50:50, and 75:25 at ϵ_{HB} = 6−12 kT in simulations using the *Atomistic informed CG Config -1 model*. For each simulation, we compute the H-bonding propensity from ten configurations collected. Error bars represent the standard deviation of these means across the three independent trials.

Distribution of angle between the H-bonding chains for the mixture of: (A) [0.6 d] and [0.8 d] (B) [0.6 d] and [1.5 d] across the mixture compositions of 25:75, 50:50, and 75:25 at ϵ_{HB} =12kT using the *Atomistic informed CG Config -1 model.* For each simulation, we compute the distribution of angles between the H-bonding chains from ten configurations collected. Error bars represent the standard deviation of these means across the three independent trials.

►Using older model (Figures S26- S29)

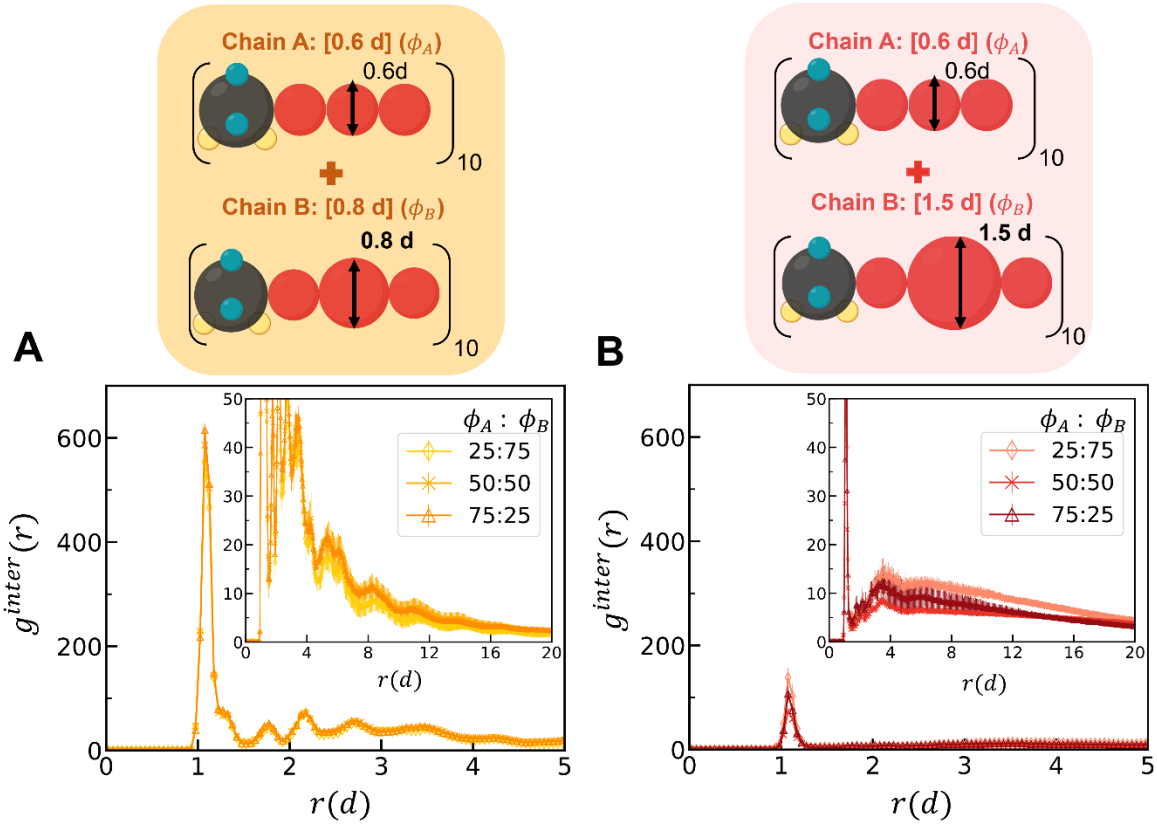

Figure S26: Inter-chain sulfamide-sulfamide RDFs ($g^{inter}(r)$) using **older CG model** for mixture of (A) [0.6 d] and [0.8 d] (B) [0.6 d] and [1.5 d] for mixture compositions of 25:75, 50:50 and 75:25 at ϵ_{HB} = 12 kT. Inset display $g^{inter}(r)$ (on y-axis) for r >20d (on x-axis), highlighting the long-range spatial organization. For each simulation, we compute the RDFs from ten configurations collected. Error bars represent the standard deviation of these means across the three independent trials.

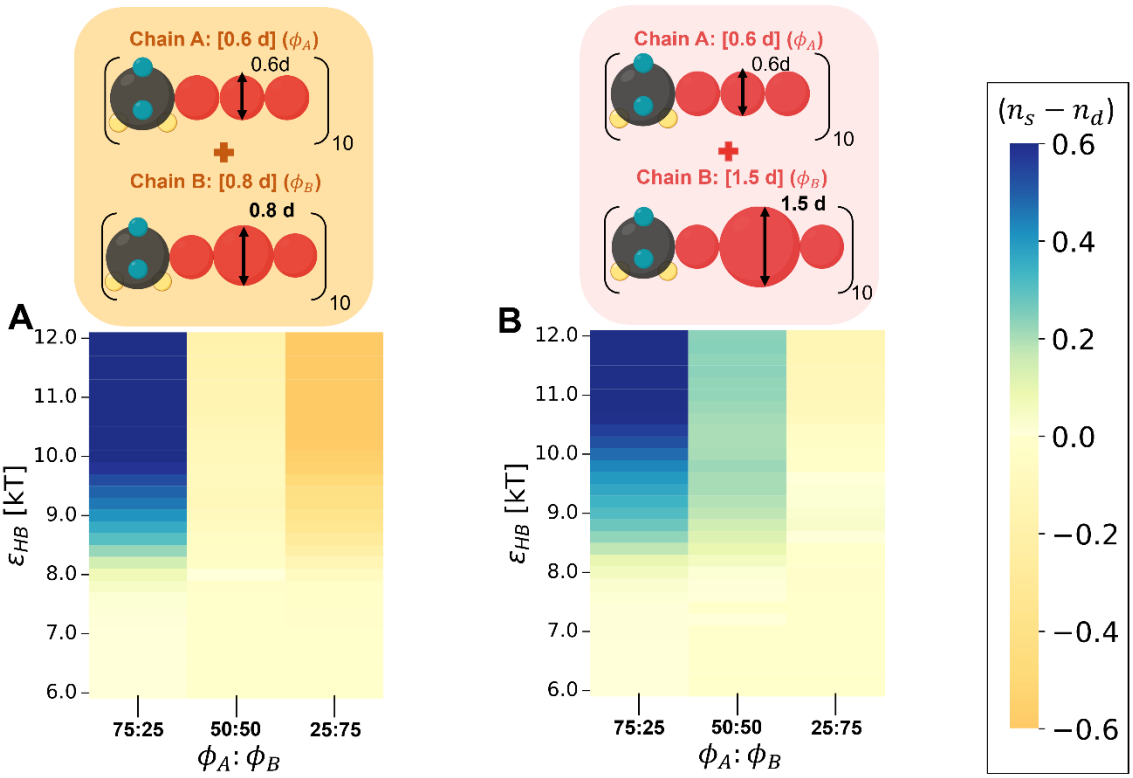

Figure S27: Heat maps showing the difference in hydrogen bonding between identical chain types (n_s) and different chain types (n_d) using the **older CG model** for the two mixtures (A) [0.6 d] and [0.8 d] (B) [0.6 d] and [1.5 d] - at varying H-bonding strengths (y-axis) and mixture compositions (x-axis).

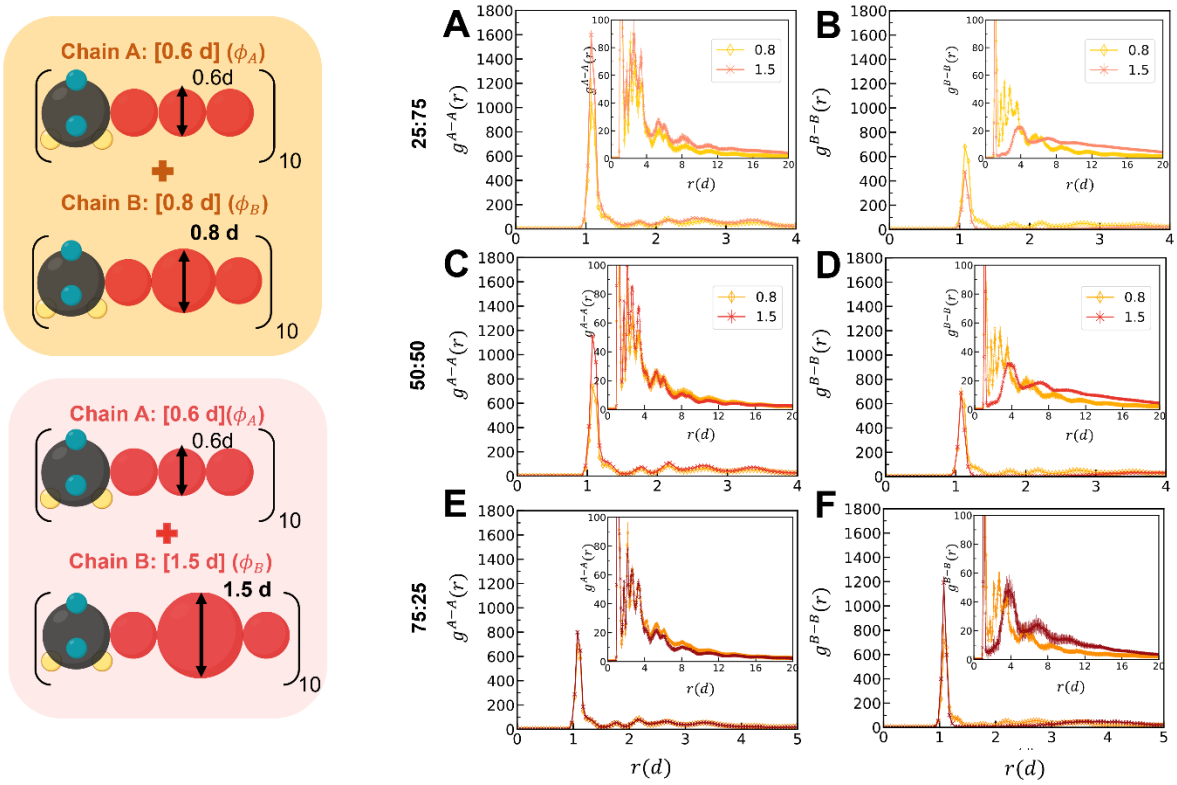

Figure S28: Sulfamide-sulfamide RDFs using the **older CG model** are shown for mixtures at different mixture compositions: (A, B) at 25:75, (C, D) at 50:50, and (E, F) at 75:25 at ϵ_{HB} = 12 kT. (A, C, E) shows $g^{A-A}(r)$ while (B, D, F) show $g^{B-B}(r)$. (A, C, E) shows $g^{(A-A)}$ (r) while (B, D, F) show $g^{(B-B)}$ (r). The yellow shading represents the mixture of [0.6 d] and [0.8 d], the red shading represents [0.6 d] and [1.5 d]. For each simulation, we compute the RDFs from ten configurations collected. Error bars represent the standard deviation of these means across the three independent trials.

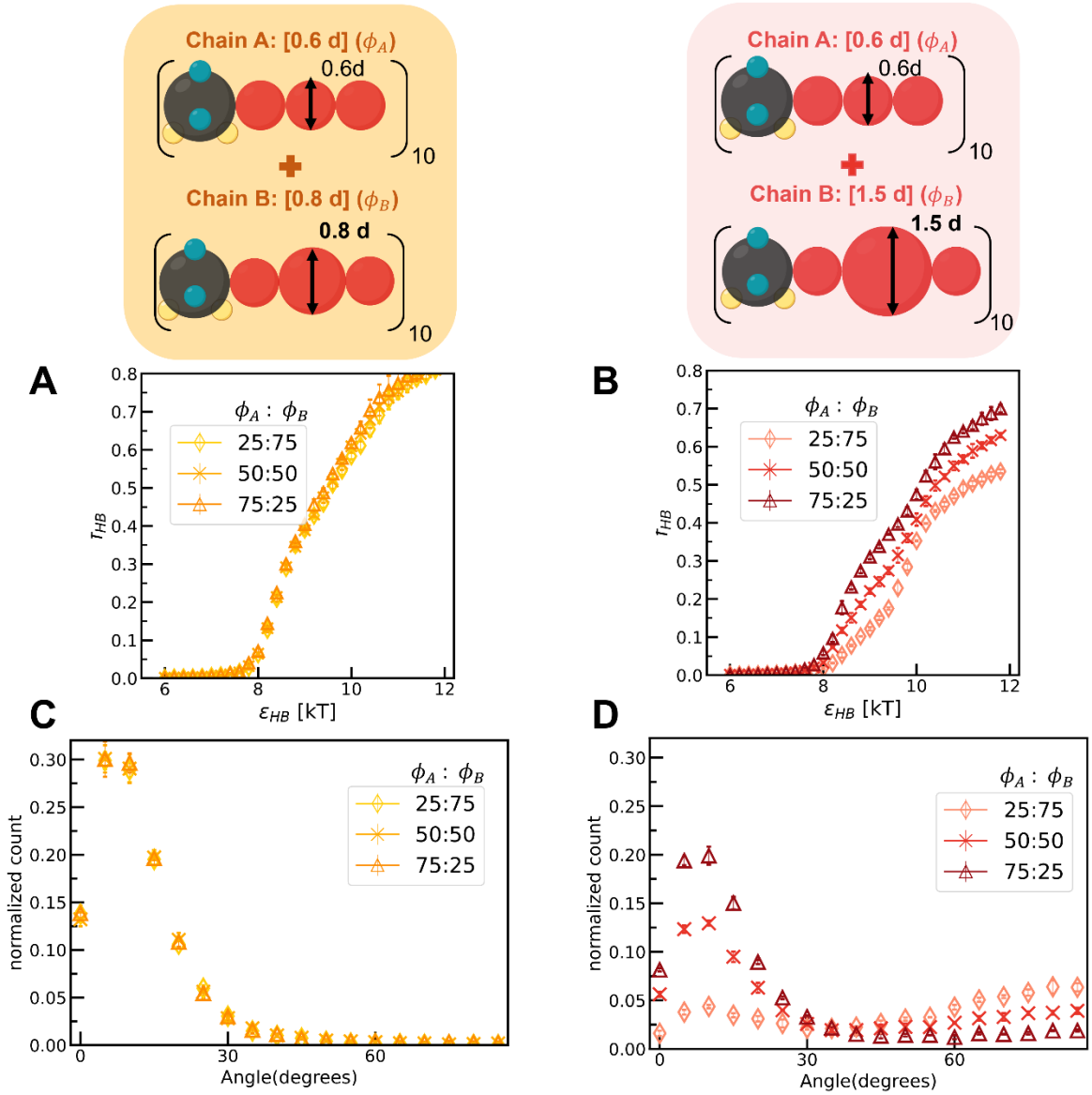

Figure S29: H-bonding propensity (f_{HB}) for mixture of: (A) [0.6 d] and [0.8 d] (B) [0.6 d] and [1.5 d] across the mixture compositions of 25:75, 50:50, and 75:25 at ϵ_{HB} = 6−12 kT in simulations using the **older CG model**. For each simulation, we compute the H-bonding propensity from ten configurations collected. Error bars represent the standard deviation of these means across the three independent trials.

Distribution of angle between the H-bonding chains for the mixture of: (A) [0.6 d] and [0.8 d] (B) [0.6 d] and [1.5 d] across the mixture compositions of 25:75, 50:50, and 75:25 at ϵ_{HB} =12kT using the **older CG model**. For each simulation, we compute the distribution of angles between the H-bonding chains from ten configurations collected. Error bars represent the standard deviation of these means across the three independent trials.

References:

1. Z. Wu, J. W. Wu, Q. Michaudel and A. Jayaraman, *Macromolecules*, 2023, **56**, 5033–5049.
2. B. Gong, C. Zheng, E. Skrzypczak-Jankun and J. Zhu, *Org Lett*, 2000, **2**, 3273-3275.